Climate Dynamics (2001) 17: 259–276

K. E. Trenberth · J. M. Caron · D. P. Stepaniak

The atmospheric energy budget and implications for surface fluxes and ocean heat transports

Received: 21 March 2000 / Accepted: 21 June 2000

Abstract Comprehensive diagnostic comparisons and evaluations have been carried out with the National Centers for Environmental Prediction/National Center for Atmospheric Research (NCEP/NCAR) and European Centre for Medium Range Weather Forecasts (ECMWF) reanalyses of the vertically integrated atmospheric energy budgets. For 1979 to 1993 the focus is on the monthly means of the divergence of the atmospheric energy transports. For February 1985 to April 1989, when there are reliable top-of-the-atmosphere (TOA) radiation data from the Earth Radiation Budget Experiment (ERBE), the implied monthly mean surface fluxes are derived and compared with those from the assimilating models and from the Comprehensive Ocean Atmosphere Data Set (COADS), both locally and zonally integrated, to deduce the implied ocean meridional heat transports.

While broadscale aspects and some details of both the divergence of atmospheric energy and the surface flux climatological means are reproducible, especially in the zonal means, differences are also readily apparent. Systematic differences are typically $\sim$20 W m^{-2}. The evaluation highlights the poor results over land. Land imbalances indicate local errors in the divergence of the atmospheric energy transports for monthly means on scales of 500 km (T31) of 30 W m^{-2} in both reanalyses and $\sim$50 W m^{-2} in areas of high topography and over Antarctica for NCEP/NCAR. Over the oceans in the extratropics, the monthly mean anomaly time series of the vertically integrated total energy divergence from the two reanalyses correspond reasonably well, with correlations exceeding 0.7. A common monthly mean climate signal of about 40 W m^{-2} is inferred along with local errors of 25 to 30 W m^{-2} in most extratropical regions. Except for large scales, there is no useful common signal in the tropics, and reproducibility is especially poor in regions of active convection and where stratocumulus prevails. Although time series of monthly anomalies of surface bulk fluxes from the two models and COADS agree very well over the northern extratropical oceans, the total fields all contain large systematic biases which make them unsuitable for determining ocean heat transports. TOA biases in absorbed shortwave, outgoing longwave and net radiation from both reanalysis models are substantial (>20 W m^{-2} in the tropics) and indicate that clouds are a primary source of problems in the model fluxes, both at the surface and the TOA. Time series of monthly COADS surface fluxes are shown to be unreliable south of about 20°N where there are fewer than 25 observations per 5° square per month. Only the derived surface fluxes give reasonable implied meridional ocean heat transports.

K. E. Trenberth (✉) · J. M. Caron · D. P. Stepaniak
National Center for Atmospheric Research,
P. O. Box 3000, Boulder, CO 80307, USA
E-mail: trenbert@ucar.edu

1 Introduction

With improvements in global analyses in recent years, especially as they have become more internally consistent with time through the various reanalysis projects, the prospects have improved for determining the interannual and perhaps longer term variability in more than just the monthly mean variables. Particular interest exists in the extent to which the depictions of the atmosphere in the analyses can throw light on the global flows of mass, moisture and energy. This paper reports on extensive computations of the atmospheric energy budgets from two sets of reanalyses, and how well they agree in their means and time sequences. It evaluates them using physical constraints where possible as well as comparisons with other products.

The mass of dry air in the atmosphere is essentially conserved and this acts as a constraint which can be exploited. In fact the global 6-hourly analyses do not conserve mass, and because transport of moisture and energy necessarily involve mass flows, it is essential to

invoke this constraint to be able to make any sense of the budgets of these other quantities (Trenberth 1991, 1997, Trenberth and Solomon 1994). Moisture budgets can be checked to some extent through computations of the vertically integrated moisture tendencies and moisture divergence, which are balanced by evaporation E minus precipitation P (e.g., see Trenberth and Guillemot 1995, 1998). Independent estimates of the latter now exist and both quantities are separately estimated from short model integrations in association with the analyses. Energy budgets depend upon both the mass and moisture budgets, and thus it is more difficult to obtain reasonable estimates. The main prospects for checks are through vertically integrated budgets and the implied fluxes through the top and bottom of the atmosphere, see for example Curry et al. (1999) for the Tropical Oceans Global Atmosphere (TOGA) Coupled Ocean-Atmosphere Response Experiment (COARE) intensive observation period (IOP). At the surface, net fluxes should be close to zero for the long term means over land, while for the oceans they should balance the heat transport divergence and changes in ocean heat content.

The two reanalyses are those from National Centers for Environmental Prediction/National Center for Atmospheric Research (NCEP/NCAR) (Kalnay et al. 1996) and European Centre for Medium Range Weather Forecasts (ECMWF) (Gibson et al. 1997). The datasets are described in Sect. 2 along with a summary of evaluations of relevant aspects of them. The full resolution data four-times daily on model coordinates are used to obtain the best accuracy possible for 1979 to 1993. Model level analyses not only have much greater vertical and horizontal resolution than pressure coordinate analyses but they accurately resolve the surface, which is critical for vertical integrals. The NCEP/NCAR reanalyses have been used to deduce the diabatic heating by Yanai and Tomita (1998), but they used the pressure level archive and only twice daily values, so that the semidiurnal tide is aliased in their results. Yu et al. (1999) have used both NCEP/NCAR and ECMWF reanalyses to compute zonal mean atmospheric energy transport divergences but they also use pressure level analyses on a 2.5° grid.

A global atmospheric energy budget using ECMWF operational analyses was described in detail by Trenberth and Solomon (1994), and the general framework for such studies was spelled out more fully in Trenberth (1997). Trenberth (1998) reported on results from NCEP/NCAR reanalyses, especially insofar as they provided new estimates of poleward heat transport by the oceans, but it is only now that we are in a position to compare the results from the two centers and thereby provide an assessment of reproducibility and thus confidence in the results. Hence, the reanalyses have been used to compute the vertically-integrated mass, moisture, heat, and energy budgets for the atmosphere. Details of the extensive computations are given in the appendix. The vertically integrated atmospheric energy budget is computed from the changes in energy storage and the divergence of the energy transport by the atmosphere, using the methods and the mathematical framework outlined in Sect. 3 and the results are given in Sect. 4. These terms must be balanced by the combination of the net surface fluxes and net fluxes through the top-of-the-atmosphere (TOA). The latter are measured by satellite and vary by relatively small amounts from year to year. Therefore the analysis also focuses on a subperiod from February 1985 to April 1989 when there are reliable TOA radiation data from the Earth Radiation Budget Experiment (ERBE), which are also described in Sect. 2. Indirect estimates are made of the total surface flux as a residual of the TOA satellite observed net radiation and the divergence of the energy transports from global atmospheric analyses. These are referred to as "derived fluxes". While many previous studies, reviewed in Trenberth and Solomon (1994), have performed zonal mean atmospheric heat budget computations, heat budgets have not been done locally or with consistent TOA radiation.

The net surface fluxes consist mainly of the sensible, latent and radiative fluxes, with additional small components of sensible heat associated with precipitation. Independent estimates exist of these quantities from bulk flux estimates such as from Comprehensive Ocean Atmosphere Data Set (COADS; Woodruff et al. 1987), and we make use of those from da Silva et al. (1994) in our evaluation. Comparisons are also made with alternative estimates, including those from the reanalysis models. Section 4 presents the results for the ERBE subinterval, along with the implications at the surface. The results of the intercomparisons highlight the need to evaluate the model fluxes and we do this by comparing the TOA radiative fluxes with those of ERBE. Computations of the zonal mean meridional ocean heat transports as a residual are also used as a diagnostic, assuming no changes in ocean heat storage. Section 4 also presents the implied meridional ocean heat transports. Section 5 discusses the results and summarizes the conclusions.

2 Data

2.1 Reanalyses

The reanalyses from NCEP/NCAR and ECMWF have been used to compute the detailed atmospheric budgets of several quantities. The period examined is that of the common data from 1979 to 1993. The global analyses are produced on model (sigma or hybrid) surfaces which consist, in simplest form, of a sigma (σ) terrain-following coordinate in which the lowest level corresponds to $p = p_s$, where p is pressure, p_s is the surface pressure and $\sigma = p/p_s$. Hybrid η coordinates consist of σ near the surface but with a gradual transition to pressure with height. Model coordinates are strongly preferred if vertical integrals are performed because the integrals are as accurate as possible and the lower boundary conditions are more easily handled than in p coordinates.

In the process of generating the reanalyses, forecasts are made to act as the first guess for the subsequent analysis, and several model-derived quantities are computed and archived that are of

interest. In particular, the net surface fluxes and the sensible, latent and radiative components are computed along with the TOA radiative fluxes, and these will be used for comparison with the ERBE data and derived surface fluxes. Here we use the first 6-hour accumulated fluxes from NCEP and the 12–24 hour accumulated fluxes from ECMWF (see below). These will be referred to as "NCEP model" and "ECMWF model" fluxes.

The NCEP system is based on a numerical weather prediction model with T62 spectral resolution and 28 sigma levels in the vertical with five of those levels in the atmospheric boundary layer. The Spectral Statistical Interpolation scheme is employed in the analysis with complex quality control. Fields are not initialized. An evaluation of some aspects of the NCEP/NCAR reanalyses from the standpoint of moisture transport is given by Mo and Higgins (1996). They note that there is very little spinup between 0–6 h and 12–24 h forecast values of the NCEP model evaporation although there is some precipitation spinup of 0.1 to 0.2 mm/day, with maxima in the tropics. For convenience we refer to these as the NCEP reanalyses.

There was a problem with the NCEP/NCAR reanalyses which affects the quality of the reanalyses over the Southern Hemisphere (SH). The problem arose from the assimilation of PAOBS (see http://wesley.wwb.noaa.gov/paobs/paobs.html) in which the observations were erroneously shifted by 180° in longitude affecting 1979–1992 (14 years). PAOBS are produced by the Australians for the data poor southern oceans and are the product of human analysts who estimate sea-level-pressure based on satellite data, conventional data, and time continuity. Tests run on the impact of the problem indicate (i) the SH middle and high latitudes (40°–60°S) are most affected, (ii) the SH winter months are affected more than the SH summer months; (iii) the differences decrease rapidly as the time-scale increases from synoptic to monthly. Unfortunately, this problem is likely to affect both the model and derived fluxes over the southern oceans.

The ECMWF reanalyses (ERA-15) are at T106 resolution with 31 levels in the vertical and a hybrid coordinate that transitions to a pressure coordinate above about 100 mb. Of note is that a diabatic, nonlinear normal mode initialization was applied. Evaluations of performance of the system are given by Uppala (1997) and Kållberg (1997). The latter notes the significant spin up in the first 24 hours so that the fluxes are better taken from a more extended model run. We use the 12–24 hour values, as suggested by Kållberg (1997), but at the expense of increased model bias and less analysis influence. Stendel and Arpe (1997) compare the hydrological cycles at different times during the spin up.

A comprehensive evaluation of the vertical structure and annual cycle of mass budget as seen through the large-scale divergent circulation from reanalyses from both centers is given in Trenberth et al. (2000). It is shown that the mean annual cycle is reasonably reproduced in both reanalyses, thereby providing a new level of confidence in the results compared with results from operational analyses. The aforementioned analysis of the mass fluxes and vertical structures of the large-scale overturning includes such components as the Hadley and Walker circulations. However, the results also show that the vertically integrated mass budgets contain large errors which have to be adjusted for in the computations before reliable results can be achieved.

Comprehensive evaluation of the moisture budget from NCEP reanalyses was given by Trenberth and Guillemot (1998) who concluded that there was a negative bias in tropical precipitation which was probably an indication that the divergent circulation is too weak. A comparison of the moisture budgets in both reanalyses by Stendel and Arpe (1997) concluded overall that the ECMWF reanalysis precipitation fields were superior to those of other reanalyses when compared with Global Precipitation Climatology Project (GPCP) observational data. Annamalai et al. (1999) also found the ECMWF reanalyses to be superior in describing the summer Asian monsoon. However, over South America, Kållberg (1997) traced major analysis problems in western Amazonia to how the semidiurnal tide was dealt with, and its interactions with the soil moisture relaxation and assimilation method for humidity. This problem was discovered while analysing 1986, and so a fix of removing synop surface pressure observations from the analysis was included by ECMWF from January 1987 onwards.

In addition, there are continuity problems with the ECMWF reanalyses arising from the positive reinforcement of biases in satellite radiances with those of the assimilating model first guess (Trenberth et al. 2001). Two spurious discontinuities are present in tropical temperatures with jumps to warmer values throughout the tropics below 500 mb in late 1986 and early 1989, and further spurious interannual variability is also present. These features are also reflected in the specific humidity fields. The temperature discrepancies, which were identified initially using microwave sounder unit data, have a complex vertical structure with height (warming below 500 mb but cooling in the layer above) and these problems affect moist static energy profiles and therefore poleward heat transports. These changes also contribute to the substantial problems regionally in the hydrological cycle over Africa (Stendel and Arpe 1997). The time series of tropical temperatures from the NCEP reanalyses appear to be more consistent than those from ECMWF.

In processing the data, for convenience we first transform the NCEP reanalyses to T63 resolution by adding a zero coefficent for the extra mode. For fields which have significant variance at the truncation limit, such as divergences, this introduces ringing effects and highlights the fact that the true resolution of the reanalyses is less than T62. When products are taken with such fields, experience shows that computational noise is present for waves beyond about T42. For instance, for the energy divergence, wavenumber spectra typically fall off slightly in power beyond about total wave number 15 to wave 42, but then exhibit an increase which peaks at T63 in the NCEP reanalyses. Noise also occurs in the ECMWF analyses. Accordingly, all fields are truncated with a tapered filter at T42 resolution before generating comparisons and analysis of variance. The filter is applied in spectral space; at T31 it has a response function of 0.93, the half power point (amplitude response 0.71) is at T36, and at T42 the response function is 0.37 $\left(\frac{1}{e}\right)$. The results are smoothed to T31 or T21 resolution for plotting purposes.

It should be noted that there is no requirement for the reanalyses to satisfy physical constraints. While such constraints are satisfied by the assimilating model, the introduction of the analysis increments every six hours upsets the balances because of model biases. For instance, in the NCEP reanalyses, over the southeastern United States in summer, analysis increments systematically moisten the atmosphere only to be balanced by precipitation in the model owing to the inability of the model to sustain the observed high levels of humidity (Trenberth and Guillemot 1998).

2.2 TOA radiation

From 1985 through early 1989 the ERBE mission provides the best estimates of the TOA radiation budgets. This is also a period of considerable interest because of the 1986–87 El Niño and the subsequent 1988–89 La Niña. Estimates of errors from satellite measurements of TOA radiation from ERBE were reviewed by Trenberth and Solomon (1994). There is a root mean square (rms) uncertainty estimate of 7.8 W m^{-2} for the three satellite combination versus 11 W m^{-2} for one satellite, with larger uncertainty in the absorbed solar radiation (ASR). The ERBE data contain discontinuities when the NOAA-9 satellite was lost, and we have adjusted the dataset to accommodate this. We have also filled in missing data, which is pervasive near the delimiter of the solar radiation. Trenberth (1997) describes the methods, changes and availability of the revised ERBE dataset (see www.cgd.ucar.edu/cas/catalog).

A comparison by Yang et al. (1999) of NCEP reanalysis radiation products with two years of ERBE data (1985 and 1986) found good agreement with clear sky solar radiation but too much reflected solar radiation for the all sky case (by 12.6 W m^{-2}), and indicated problems with clouds and moisture. Outgoing Longwave Radiation (OLR) differences were strongly seasonal and reanalysis values were 1.5% too high overall. The comparison indicated severe problems in areas of complex topography. Indeed, the surface albedo

over land, and especially over the Sahara desert was found to be too low. These problems have implications for model-derived quantities but not necessarily for the atmospheric diagnostics we compute.

2.3 COADS data

Recent global air-sea flux climatologies based on ship data and bulk formulae (da Silva et al. 1994, Josey et al. 1999) exhibit an overall global imbalance; on average the ocean gains heat at a rate of about 30 W m^{-2}. This was adjusted by da Silva et al. (1994) by globally scaling their flux estimates. As Josey et al. (1999) found good agreement with buoy measurements in their unadjusted flux estimates, the evidence suggests that spatially uniform corrections are not appropriate but should be done locally. We used the adjusted values in this study, although, as we shall see, the adjustments do not balance the global ocean heat budget for the ERBE period.

3 Methods and physical framework

The general physical framework and mathematical expressions, including the apparent heat and moisture sources, are given in Trenberth (1997) and the equations relevant here are given below.

3.1 Vertical integrals

The mass weighted vertical integral of any quantity M integrated in the vertical over the mass of the atmosphere from the bottom ($p = p_s$, $z = 0$) to the top ($p = p_t = 0$, $z = \infty$) is given by

$$\widetilde{M} = \int_0^\infty \rho M \, \mathrm{d}z = \frac{1}{g}\int_{p_t}^{p_s} M \, \mathrm{d}p = \frac{1}{g}\int_{\eta_s}^{\eta_t} \frac{\partial p}{\partial \eta} M \, \mathrm{d}\eta \tag{1}$$

where these refer to geopotential height, pressure and hybrid model coordinates and η_t and η_s correspond to $p = p_t$ and $p = p_s$. The $\frac{\partial p}{\partial \eta}$ plays the role of a density factor in these coordinates. In the event that σ is the vertical coordinate, this mass-weighting factor becomes p_s.

In computing monthly means, the most accurate result is achieved if the vertical integral is computed each time and averaged. Computing a single vertical integral for each month using the monthly mean field of $\widetilde{M}$ – which can be a cross product or covariance – and mean surface pressure as the coordinate basis and lower limit of integration, ignores the covariances of $\widetilde{M}$ with p_s and makes only small and acceptable errors (Trenberth et al. 1993). The lower boundary condition in model coordinates is $\dot{\eta} = 0$, and in p-coordinates is $\omega_s = \frac{\partial p_s}{\partial t} + \mathbf{v}_s \cdot \nabla p_s$, at $p = p_s$.

3.2 Monthly means and tendencies

Convention has the monthly mean as the average of the values from 00 UTC on the first day to 18 UTC last day of each month; effectively the monthly mean begins and ends at 21 UTC on last day of each month. Therefore to do monthly budgets, we compute the tendency terms of the changes in storage of the quantities of interest for each month using average quantities from 18 UTC last day and 00 UTC first day of next month.

3.3 Mass budget

In carrying out budgets of any atmospheric quantity, the values are mass weighted, which places a premium on the requirement for the mass budget to be satisfied. Calculations of the mass budget using atmospheric data on pressure levels reveal that mass is not conserved by the analyses (Boer and Sargent 1985, Alexander and Schubert 1990, Trenberth 1991, Trenberth et al. 1995) and this lack of conservation constitutes a major error component in the other budgets. Trenberth (1991, 1997) present the approach used here to adjust the velocity fields so that surface pressure tendencies for monthly means are balanced exactly. In all of our results, we find that the mass budget is much more nearly in balance in the ECMWF reanalyses, where the imbalances presumably result primarily from the 6-hour sampling, than for NCEP where the much larger imbalances presumably arise from lack of initialization; see Trenberth (1997) for examples.

For total mass the appropriate balance is

$$\frac{\partial p_s}{\partial t} + \nabla \cdot \int_o^{p_s} \mathbf{v} \, \mathrm{d}p = g(E - P). \tag{2}$$

In meteorology the right-hand side is typically ignored but this could contribute to heat budget errors of about 10 W m^{-2} (Trenberth 1997). For water vapor

$$\frac{\partial w}{\partial t} + \nabla \cdot \frac{1}{g}\int_o^{p_s} q \, \mathbf{v} \, \mathrm{d}p = E - P \tag{3}$$

where the precipitable water $w = \frac{1}{g}\int_o^{p_s} q \mathrm{d}p$. E is the rate of evaporation and P is precipitation rate per unit mass, and we have ignored other forms of liquid and frozen water in the atmosphere.

3.4 Heat and energy transports

Energy in the atmosphere is in the form of kinetic energy k, internal energy $I = c_v T$, and potential energy P_e, where c_v is the specific heat at constant volume, and $I + k + P_e$ is conserved in the absence of heating and friction when integrated over the entire mass of the atmosphere. Vertically integrating and combining the dry and moist energy equations through the atmospheric column, gives

$$\frac{\partial}{\partial t}\frac{1}{g}\int_o^{p_s} (c_p T + k + Lq + \Phi_s)\mathrm{d}p + \nabla \cdot \frac{1}{g}\int_o^{p_s} (h + k)\mathbf{v} \, \mathrm{d}p = R_T + F_s \tag{4}$$

where $s = c_p T + \Phi$ is the dry static energy, c_p is the specific heat at constant pressure, $h = s + Lq$ is the moist static energy. Also, R_T is the net downward radiation through the TOA and F_s is the net upward flux through the surface.

The first term in (4) is the change in storage in the atmosphere of internal, potential, kinetic, and latent energy. The total atmospheric energy transport is given by

$$\mathbf{F}_A = \frac{1}{g}\int_o^{p_s} (h + k)\mathbf{v} \, \mathrm{d}p \; . \tag{5}$$

The second term in (4) then is the total atmospheric energy transport divergence. In a steady state, or ignoring the tendency terms which are small for time averages, from (4)

$$\nabla \cdot \mathbf{F}_A = R_T + F_s \tag{6}$$

is the equation describing the transport link from source to sink.

We compute the right hand side of (4) as a residual using the full reanalysis datasets in model coordinates, and include full computation of the tendency terms for each month. The largest part of the mass correction involves subtracting $\frac{1}{g}(\widetilde{h} + \widetilde{k}) \times (2)$ from the raw computation. Since this expression is supposed to be zero, but typically is not, the residual corrects most of the vertically integrated spurious mass balance contribution to the energetics balance.

3.5 Surface budget

On an annual mean basis, the changes in storage terms are small and often negligible, so that (6) holds. Over land, ignoring heat stored in the ground, F_s should be close to zero for the annual mean, so

$$\nabla \cdot \mathbf{F}_A^{\mathrm{land}} = R_T \tag{7}$$

and the balance lies between the atmospheric energy divergence and the net TOA radiation. Over the oceans, given estimates of R_T from satellite measurements, then F_s can be estimated as a residual from (4) and compared with independent estimates made using bulk flux formulations of the surface fluxes. Within the ocean, again ignoring heat storage changes,

$$\nabla \cdot \mathbf{F}_O = -F_s \tag{8}$$

where $\mathbf{F}_O$ is the vertically integrated divergent ocean heat transport. This allows estimates to be made of the divergent component of the ocean heat transport. Further, integrating over the entire oceans should give a value of zero, as ocean currents are bounded, and thus the global ocean integral provides a measure of the bias.

3.6 Diagnostics

We compute energy budgets for each month. Comparison of long-term (15 year) means for each month allows the systematic differences to emerge, and the annual mean differences between the results from the two centers capture most of that component. We also use the standard deviations, correlations and rms differences of monthly anomalies as measures of the reproducibility of reanalysis results. If we assume that the variances in the two reanalyses are similar, the positive correlation comes from a common signal, and that the errors are uncorrelated and contributed by both reanalyses, then the standard deviation of the errors in each are a factor of $2^{\frac{1}{2}}$ less than the rms differences. This allows us to assess the common component, which we regard as a measure of the true signal of climate variability, as well as the noise level. We also present estimates of the zonal means, either as direct or rms averages around a latitude circle.

There is considerable high frequency (monthly) variability in the results which arises in part from partially sampled synoptic systems within a month, known as weather noise. Accordingly, for the short ERBE period, we use seasonal anomalies in the comparisons to reduce the sampling noise levels somewhat.

4 Results

4.1 1979–1993

The annual mean vertically integrated total energy divergences from NCEP and ECMWF over 1979–1993 are presented in Fig. 1 along with their difference. On most figures like this the zonal mean is given at right. The zonal means of the third panel are close to zero and therefore instead the zonal mean rms values are given. Broad aspects of the fields are similar, especially in the zonal means, with convergence in the tropical eastern Pacific and Atlantic Oceans, divergence over the subtropical oceans, peaking over the Kuroshio and Gulf Stream regions, and convergence poleward of 40°N and 40°S. Continental values, especially over Australia, Eurasia, North America, Africa and Antarctica tend to be more negative than adjacent regions. This indicates a flow of heat from the ocean to the land which is most pronounced in winter, when the moderating influence of the ocean on continental temperatures is well known (Hurrell and Trenberth 1996). Advective processes are weaker in summer in the Northern Hemisphere, and thus winter patterns dominate the annual mean. Many detailed features in Fig. 1 are also very similar, such as the divergence south of Africa in the vicinity of the retroflection region of the Agulhas current, and the convergence to the northwest. But differences are also readily apparent, especially in the magnitudes of the divergence in the western subtropical Pacific.

Zonal mean rms values of the differences between NCEP and ECMWF reanalyses (Fig. 1, panel 3) are 20 to 30 W m^{-2}. This indicates the typical magnitude of the local mean difference which is much larger over land and especially mountainous regions. One reason for this has been found for the ECMWF reanalyses in the problems discussed in section 2a over South America. Differences are also substantial over the tropical Pacific.

The standard deviation of the monthly mean anomalies for this same period (Fig. 2) are predominantly 45 to 65 W m^{-2} over the extratropical oceans in both reanalyses, and with largest values in the North Atlantic storm track. Over the tropical oceans values are slightly less than 30 W m^{-2} although ECMWF values are higher no doubt in part because of spurious variability (Trenberth et al. 2001). For annual mean standard deviations (not shown) values of about 15 W m^{-2} are about a factor of $12^{\frac{1}{2}}$ less than in Fig. 2 over the extratropical oceans, as would be expected for uncorrelated monthly anomalies, whereas values of similar magnitudes are present in the tropics owing to the greater persistence there. Over land where the net surface flux must be small on average, standard deviations are mostly less than 30 W m^{-2} for ECMWF except in the problem area of the northern Andes, whereas larger values, especially over the Himalayan-Tibetan Plateau complex and Antarctica, are evident in the NCEP standard deviations.

The reproducibility of the variability is revealed by correlations and rms differences of the monthly anomalies (Fig. 3). Correlations generally exceed 0.5 over the oceans outside of the tropics and exceed 0.75 over the North Atlantic and North Pacific, where the rms differences are less than 40 W m^{-2}. Typical rms differences are 40 W m^{-2} (see the zonal means) except that they are much higher over Antarctica and a bit less in the northern extratropics. Rms differences are generally larger over land and in the vicinity of the mountainous regions. Correlations are small and even negative in places over the tropics, especially where convection is active in the monsoons or ITCZ regions.

4.2 The ERBE period: February 1985 to April 1989

To further interpret and evaluate these results, we focus on the period for which reliable TOA radiative fluxes are available from ERBE. Annual mean statistics are computed by averaging values for each month and then averaging the twelve months. Annual means of the divergences of atmospheric energy transports (not shown) are very similar to those in Fig. 1. The net radiation flux at the TOA for this period as an annual mean is given in Fig. 4 along with the standard deviation of the monthly anomalies. The components of the ASR and OLR are given for 1988 in Trenberth and Solomon (1994). These

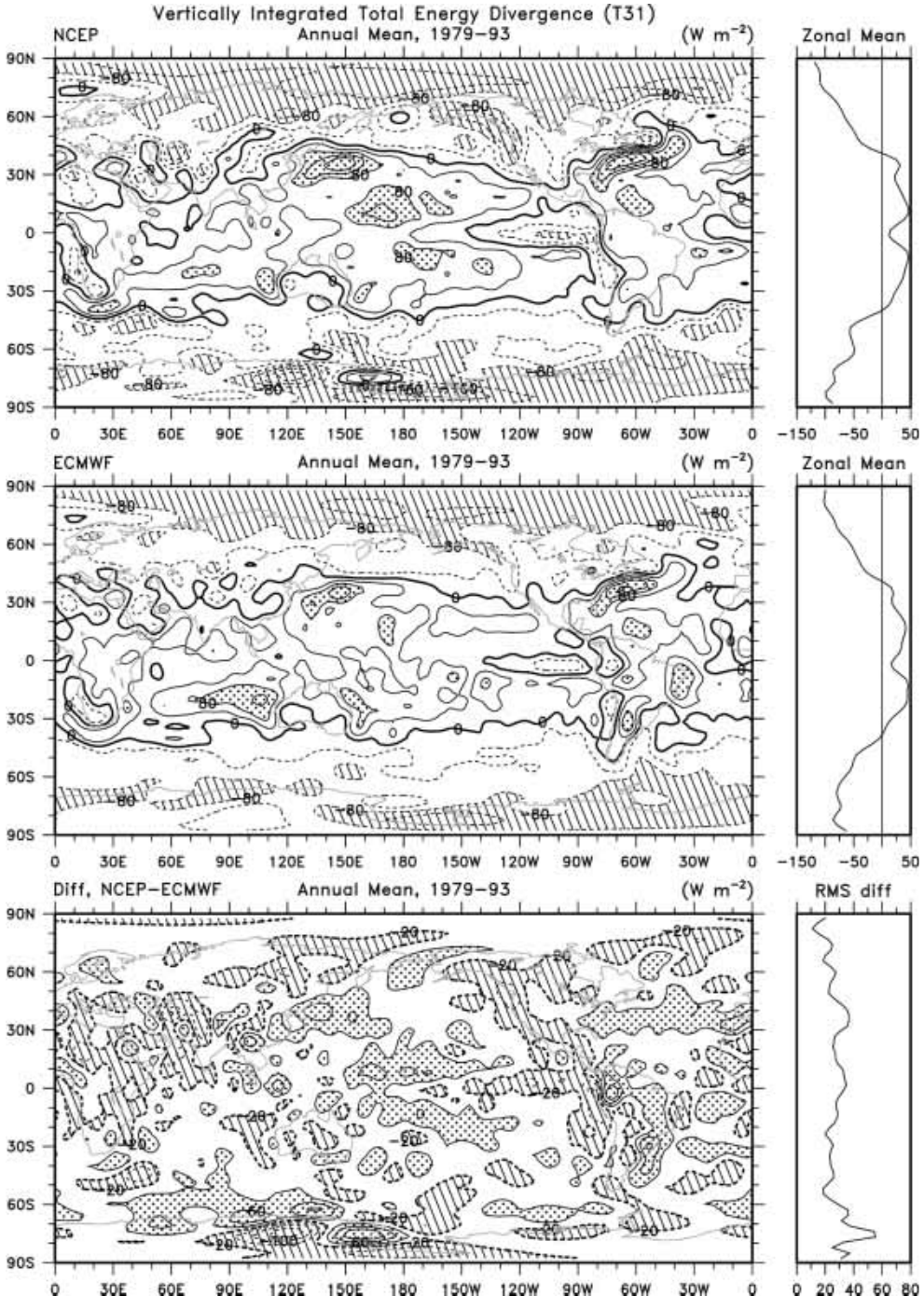

Fig. 1 Annual mean vertically integrated total energy divergence for 1979–1993 from NCEP (top) and ECMWF (center) and their difference (bottom) in W m^{-2}. The zonal mean is given at right for the top two panels and zonal mean rms value for the third panel. The fields are smoothed to T31 resolution and the contour interval is 40 W m^{-2}. For the top two panels values exceeding 80 W m^{-2} are stippled and those less than -80 W m^{-2} are hatched. In the bottom panel the contours are $\pm 20, \pm 60$ etc. Values > 20 W m^{-2} are stippled and values < -20 W m^{-2} are hatched

both show strong regional features associated with clouds, but cancellation is evident in the net radiation except in the regions of low stratocumulus decks off the coasts of California and Peru. Moreover, the latter regions also show up prominently in the standard deviations. Whereas the typical standard deviations of net TOA radiation (Fig. 4) are 5 W m^{-2}, values are as large as 15 W m^{-2} in the stratocumulus regions. Still, these values are relatively small compared with the standard deviation of the monthly mean divergence of the atmospheric energy transports, which is typically $\sim$50 W m^{-2} over the extratropical oceans (Fig. 2). Consequently, over most of the Earth, the atmospheric energy divergences are mostly compensated by the contributions at the surface.

The net radiation and the total atmospheric energy divergences are combined to produce the net surface fluxes (Fig. 5). Firstly, we focus on the values over land, which should be close to zero from (7) over such a period. We have computed both the zonal means and the

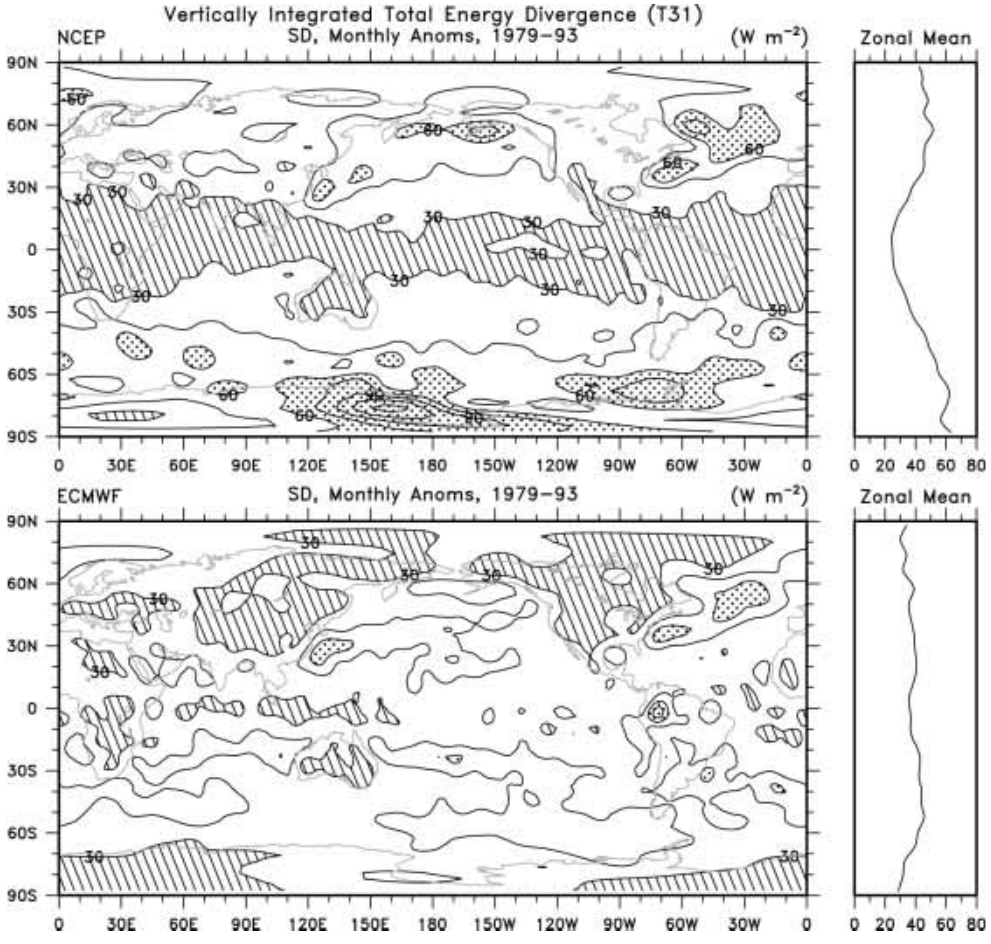

Fig. 2 Standard deviation of anomalies of monthly mean vertically integrated total energy divergence for 1979–1993 from NCEP (top) and ECMWF (bottom) in $W\,m^{-2}$. Values greater than 60 $W\,m^{-2}$ are stippled and less than 30 $W\,m^{-2}$ are hatched; the contour interval is 15 $W\,m^{-2}$

zonal mean rms values over land which are given in side panels in Fig. 5. Typical residuals for both derived surface fluxes, as shown by the rms values, are about 30 $W\,m^{-2}$ over land. This is consistent with rms differences of about 40 $W\,m^{-2}$ in Fig. 3 when it is recognized that the biggest discrepancies revealed in Fig. 3 come from the Tibetan Plateau and Andean regions where the variations are not well correlated so that a factor of $2^{\frac{1}{2}}$ applies. Thus Fig. 5 indicates that the errors in the overall monthly energy budgets of both reanalyses locally over land are about 30 $W\,m^{-2}$ (Fig. 3) but the errors are larger (often >50 $W\,m^{-2}$) in mountainous regions and over Antarctica (especially for NCEP).

Over the oceans, Fig. 3 reveals that the rms differences are somewhat smaller, and moreover, the variations are highly positively correlated. We use the assumptions given above (Sec. 3f) to assess the signal and noise in the data. For example, over the extratropical oceans typical total monthly anomaly standard deviations are about 50 $W\,m^{-2}$, the noise standard deviations are 25 to 30 $W\,m^{-2}$, and the signal standard deviations are of order 40 $W\,m^{-2}$. However, in the tropics where the correlations in Fig. 3 are less than 0.3, the noise level is about 30 $W\,m^{-2}$ and approaches that of the total field, so that any monthly signal at T31 resolution is very poorly resolved. Averaging over large regions does, however, help bring out a tropical El Niño-related signal (not shown). Also, as the total variance is higher for ERA-15 than NCEP (typically 26 vs 34 $W\,m^{-2}$) in the tropics, the noise level in ERA-15 is also higher. In part this may be because of the spurious temperature and moisture variability and discontinuities in ERA-15, discussed in Sect. 2a and documented by Trenberth et al. (2001).

A number of features are quite similar in Fig. 5. Net fluxes of energy into the ocean in the tropical eastern Pacific exceed 120 $W\,m^{-2}$ in regions where the equatorial dry zone exists, and the general absence of clouds means that solar radiation fluxes into the ocean are a maximum. Largest fluxes out of the ocean occur off the east coasts of Asia and North America over the Kuroshio and Gulf Stream, where the presence of huge sensible and latent heat fluxes in winter into the atmosphere are well established. Values exceed 150 $W\,m^{-2}$ in both reanalyses and patterns are quite similar. A number of other features are reproducible as well. These include the large fluxes into the ocean in the tropical Indian Ocean and over parts of the southern ocean, North Pacific and tropical Atlantic. Heat fluxes out of the ocean of over 60 $W\,m^{-2}$ occur on both sides of Australia and the patterns are very similar around and south of Africa.

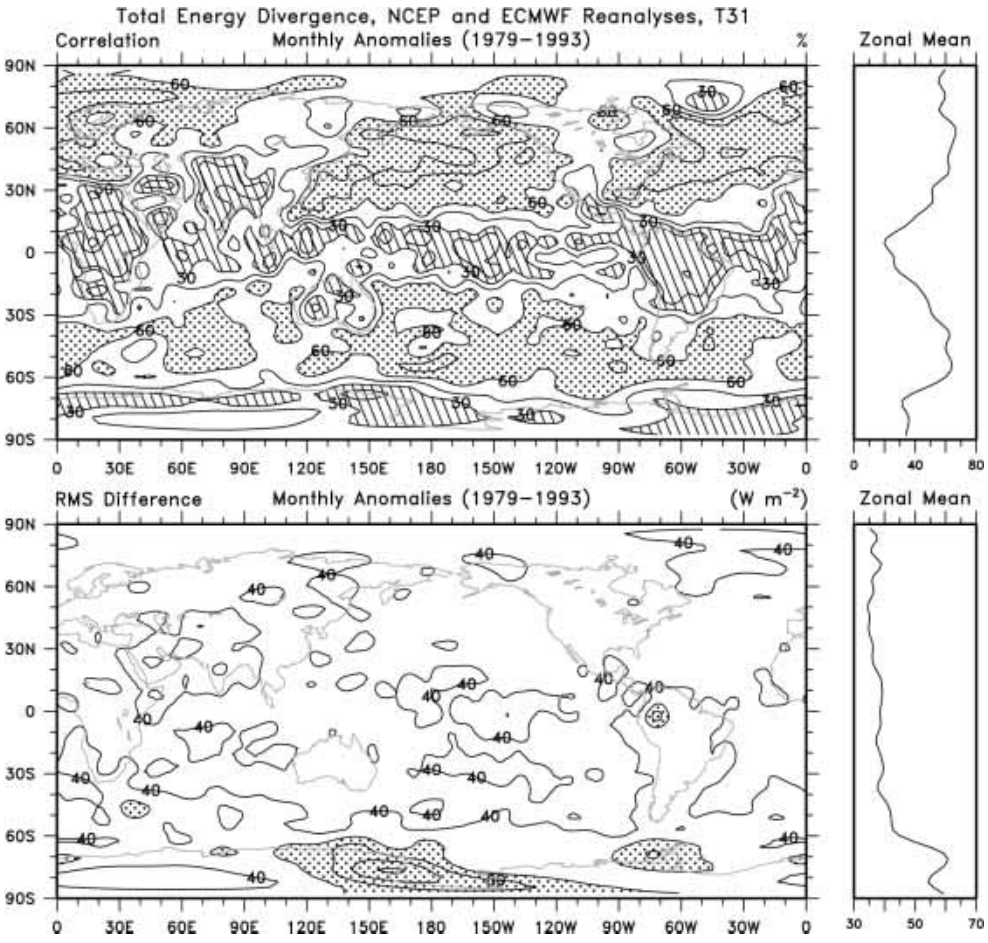

Fig. 3 For monthly NCEP and ECMWF anomalies of the vertically integrated total energy divergence for 1979–1993, given are the correlation (contour interval 15%) in % (top) and rms difference (bottom) in $W\,m^{-2}$. Correlations greater than 60% are stippled and those less than 30% are hatched. For the rms differences the contour interval is 20 $W\,m^{-2}$ beginning at 40 $W\,m^{-2}$, and values greater than 60 $W\,m^{-2}$ are stippled

4.3 Comparison with other surface fluxes

Annual means for the same period of surface fluxes from the 6-hour model integrations in the reanalyses and from COADS (da Silva et al. 1994) are shown in Fig. 6 for the ocean regions only. These can be compared with those in Fig. 5 for the derived values. Again, broad similarities exist, but details differ considerably. Before exploring these further, in order to assess their merit, we first examine the variability.

Seasonal values are somewhat more stable than monthly values, as some noise is averaged out. Therefore we present maps of standard deviations of the 16 seasonal anomalies of all 5 products in Fig. 7. This shows values of 10 to 25 $W\,m^{-2}$ over most of the oceans in the model fluxes, with some tropical Pacific patches of larger values from the ECMWF model. Somewhat larger values are apparent in the derived surface fluxes.

Anomaly correlations of the 16 seasons of the other products with COADS are given in Fig. 8. For both of the model-based products, strikingly strong correlations > 0.8 occur over the North Pacific and North Atlantic, and correlations >0.6 extend over much of the regions where there is a stronger observational base, including the Tasman Sea in the Southern Hemisphere. A similar pattern is present with the derived fluxes although the correlations are slightly smaller.

Because of the magnitude and pattern of the values south of about 20°N in Fig. 7 and some common features to all plots in Fig. 8 we examined the numbers of observations going into the COADS products. Figure 9 shows the square root of the average number of observations per 5° square, because the standard error of the mean decreases in proportion to this value (Trenberth et al. 1992). It suggests that the COADS product for monthly surface flux anomalies is unreliable over regions where there are fewer than an average of 25 observations per month per 5° square for interannual variations. Some ship tracks in the Southern Hemisphere, such as from Panama to New Zealand, and in the Tasman Sea and tropical Indian Ocean provide limited areas south of 20°N where COADS may provide useful estimates.

The zonally averaged rms differences of seasonal anomalies over the oceans (Fig. 10) exhibit large values near 65°N, which are deceptive as there is little ocean there, and attention should be directed to the values between 60°N and 60°S. The rms differences are about 20 $W\,m^{-2}$ except that values between 25 and 60°N drop to about 10 $W\,m^{-2}$ for the model versus COADS fluxes. The reproducibility among the products lends some confidence to the possibility that the temporal variations may be realistic. Fig. 11 confirms that the most promising temporal variability of the surface fluxes seems to come from the model results from the reanalyses.

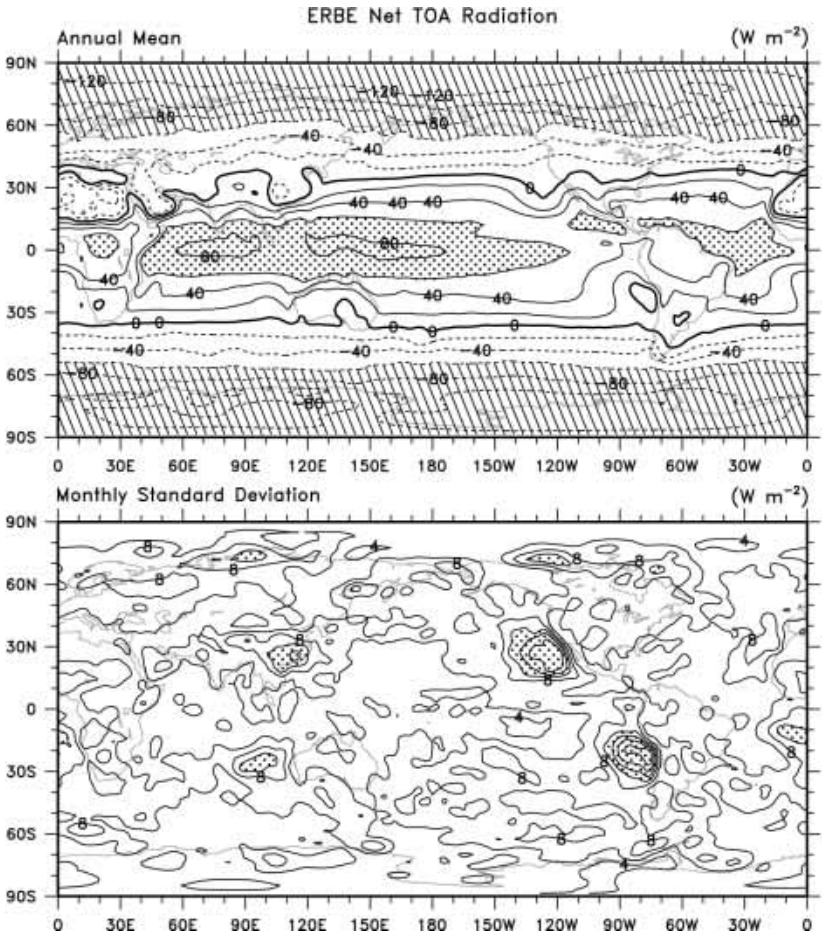

Fig. 4 Net TOA radiation for February 1985 to April 1989 from ERBE expressed as the annual mean (top) and the standard deviation of the monthly anomalies (bottom) in $W\,m^{-2}$. For the mean, values exceeding 60 $W\,m^{-2}$ are stippled, values < -60 $W\,m^{-2}$ are hatched and negative values are dashed. The contour interval is 20 $W\,m^{-2}$. For the standard deviation, the contour interval is 2 $W\,m^{-2}$ and values greater than 10 $W\,m^{-2}$ are stippled

Correlations exceed 0.8 over most of the domain outside of the tropics, with rms differences of 5 to 10 $W\,m^{-2}$, but with much larger discrepancies throughout the tropics and especially over the tropical Pacific, where rms differences exceed 20 $W\,m^{-2}$. The results in Fig. 11 can be compared with those in Fig. 3, where the correlations between the two derived products over the extratropical oceans are also quite high and often also exceed 0.8. In fact the values in Fig. 3 are much more statistically significant as there are 15 versus 4 years (14 versus 3 degrees of freedom for each season or month) and it uses monthly instead of seasonal anomalies.

Considerable caution must be exercised before accepting all of these results at face value. Reproducibility is a necessary but not sufficient requirement for building confidence. The methodologies for producing the model and COADS fluxes are all based upon bulk flux parameterizations, and the agreement is mostly a statement that the underlying meteorological fields on which they are based are very similar. Evidently this is the case where there are ample in situ observations. However, the somewhat lower level of agreement of the model and derived fields from the same assimilation system (whether NCEP or ECMWF) indicates that there are still substantial problems with physical consistency, as has been documented more generally by Yu et al. (1999).

Moreover, both of these diagnostics (Figs. 10 and 11) have the short ERBE period monthly means subtracted and so the systematic errors, such as those arising from model biases, are removed. Any biases in the parameterizations of surface fluxes, which are known to be large (Gleckler and Weare 1997), would also be removed by this process. To the extent that the biases in surface model fluxes arise from radiation, we can evaluate the TOA model fluxes by comparing them with ERBE results.

Differences of NCEP and ECMWF reanalysis model-based and ERBE ASR, OLR and net radiation for the ERBE period are substantial (Fig. 12). For ECMWF, positive biases of order 20 $W\,m^{-2}$ dominate the ASR outside of the tropics, although compensated somewhat by biases in OLR of 10 to 20 $W\,m^{-2}$ at most latitudes (note OLR is positive upwards). Thus negative biases in the net TOA radiation are in excess of 20 $W\,m^{-2}$ over the ocean in the tropics, except for the stratocumulus regions, where the bias is strongly positive. The bias is also positive over the Saharan region of Africa. For NCEP the picture is slightly

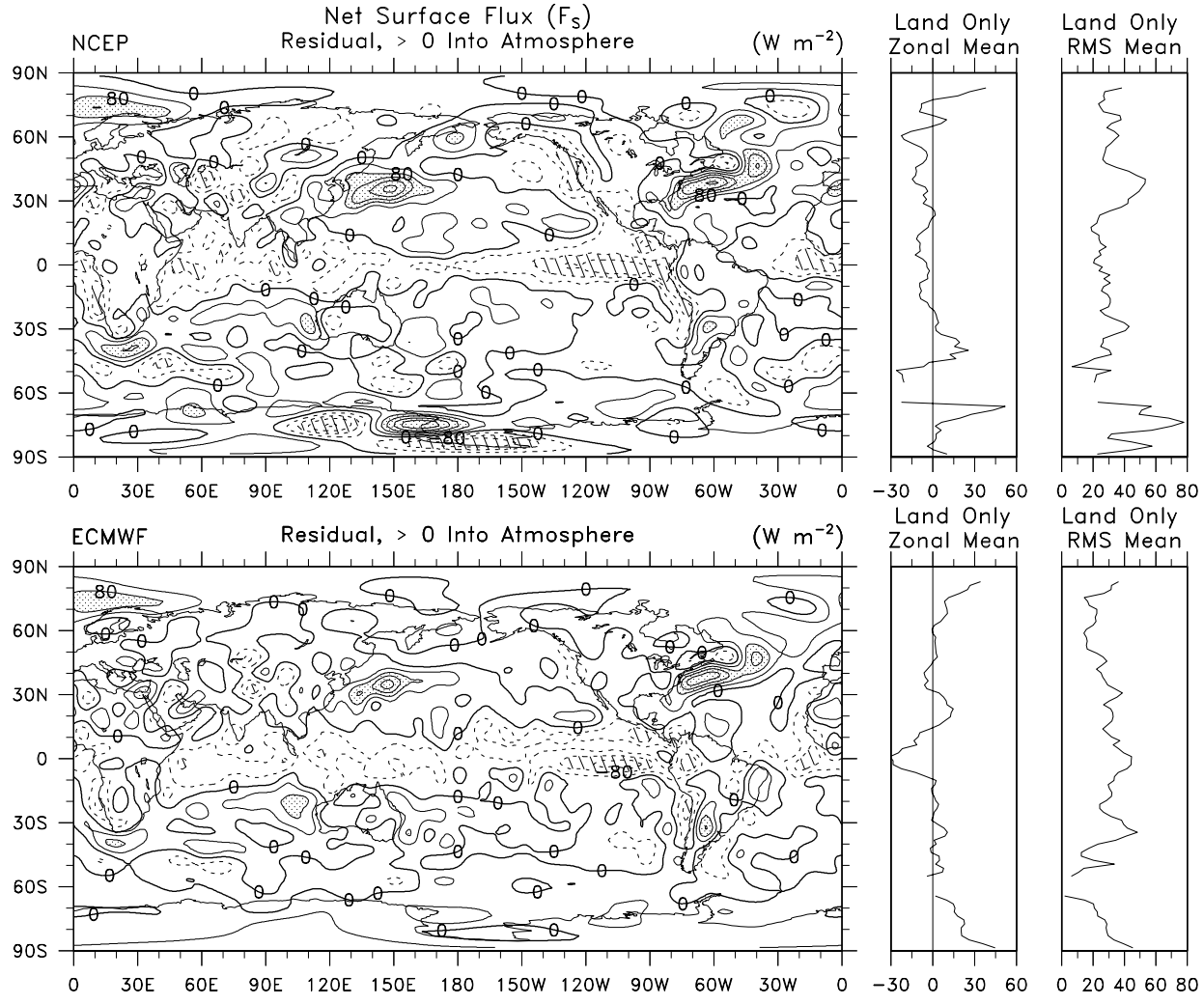

Fig. 5 Net surface fluxes derived from the total atmospheric energy divergence and TOA radiation for February 1985 to April 1989 expressed as the annual mean in W m^{-2}. Positive values are upwards into the atmosphere. Zonal means and rms values over land are given at right. Values less than −80 W m^{-2} are hatched and those greater then 80 W m^{-2} are stippled, with a contour interval of 40 W m^{-2}

better. Negative biases of order 20 W m^{-2} dominate the ASR in the tropics but are compensated to some degree by biases in OLR. Nevertheless, deficits of about 20 W m^{-2} are present throughout the tropics in the net TOA radiation. For the global means, the biases are −9.6 (4, −14) W m^{-2} for ECMWF and −11.0(−8, −4) W m^{-2} for NCEP net (ASR, OLR) radiation, where in each case the positive value is downwards.

The overall variability in both model TOA products (not shown) is similar to that given in Fig. 4 although the ECMWF model fails to capture any semblance of the maxima in the stratocumulus regions. Zonal means of the monthly anomaly correlations between net ERBE and NCEP anomalies are mostly 0.15 to 0.4, averaging around 0.3, and for ECMWF correlations range from 0.15 to 0.65, and average ∼0.45 in the northern extratropics and 0.35 in the southern extratropics, but less than 0.2 in the deep tropics. The corroboration of ECMWF anomaly values is generally much better than for NCEP outside of the stratocumulus regions.

The overall net imbalance in the ECMWF model results as shown by Kållberg (1997) at the TOA is −7.9 W m^{-2} for the first six hours of model integration and −10.1 W m^{-2} for the 18 to 24 hour integration, consistent with our values for the ERBE subperiod. The ASR spin down is largest in the tropics and is related to increases in cloud amounts. At the surface, Kållberg (1997) finds that overall there is also an ocean imbalance of +8 W m^{-2} (i.e., into the ocean) in the first 6 hours declining to −2.4 W m^{-2} from 18 to 24 hours, with the biggest change of over −6 W m^{-2} in decreases in the shortwave radiation and a significant change (−4.7 W m^{-2}) in the latent heating from 06 to 24 hours as the winds tend to increase in many places.

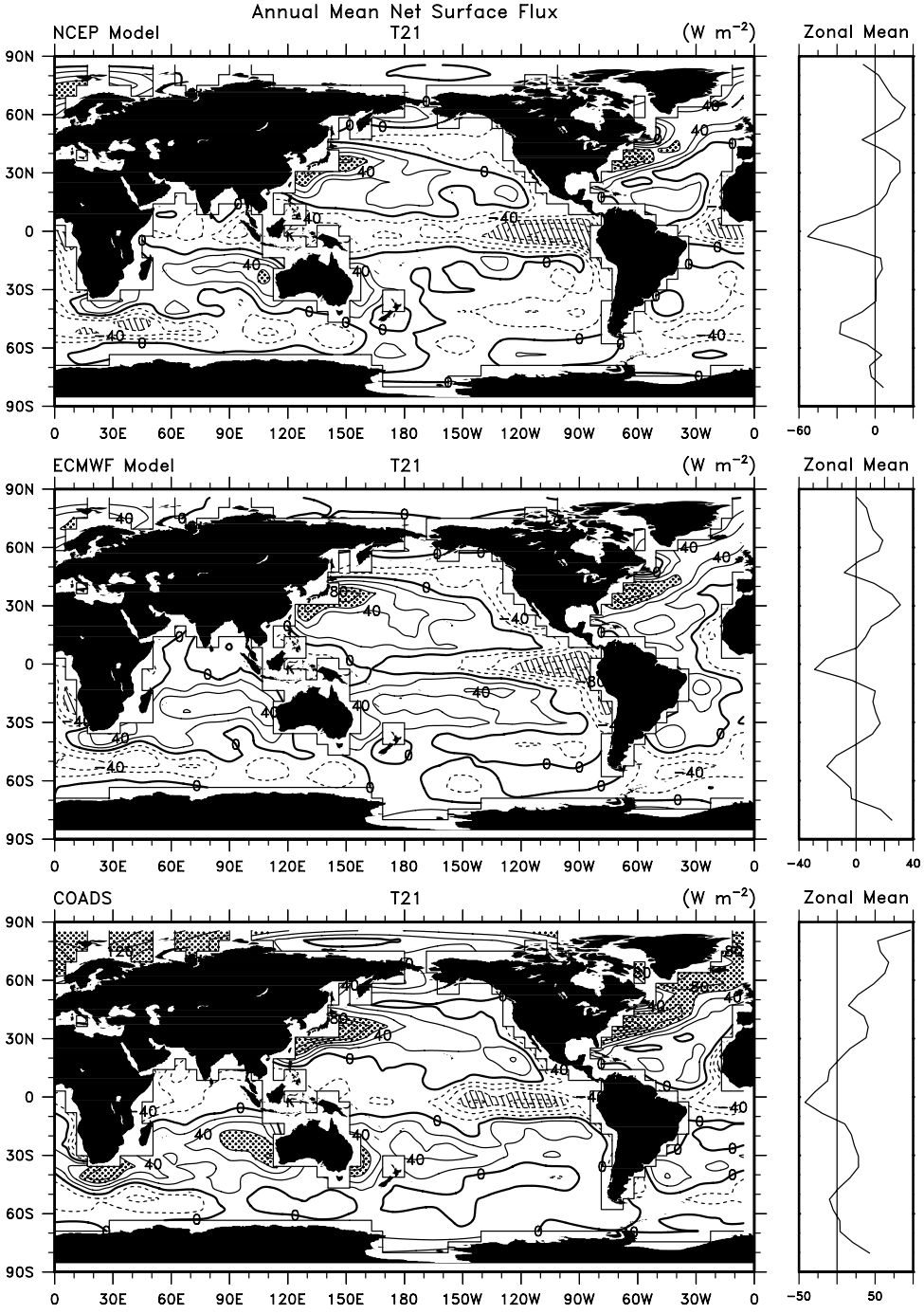

Fig. 6 Annual mean surface fluxes based upon February 1985 to April 1989 from the models for NCEP (top), ECMWF (middle) and from COADS (bottom) in W m^{-2}. The contour interval is 20 W m^{-2} and values exceeding 60 W m^{-2} are stippled and values less than −60 W m^{-2} are hatched

In general the net TOA fluxes are not very well reproduced by either center, suggesting difficulties in correctly depicting clouds. Therefore it is still not clear which method provides the best estimates of the total surface fluxes, although clearly lack of agreement means that at most one product can be correct. However, Fig. 12 shows that the model biases are significant, and only our derived values provide surface fluxes which are physically consistent with the atmospheric transports and TOA fluxes. Another way to explore this aspect is through the implied total ocean heat transport divergence.

4.4 Implied ocean heat transports

To examine the systematic biases over large areas, implied zonal mean ocean transports are computed from the surface fluxes (Fig. 13) starting at 65°N. There is a small northward ocean heat transport at 65°N of about 0.1 PW which is ignored here but included in Trenberth and Caron (2001). The accumulated bias shows up as the imbalance at the southern-most latitude, taken as 70°S owing to seasonal ice cover. The computations were done on a T42 grid (2.8°) as a compromise between the requirement for high resolution to resolve islands and

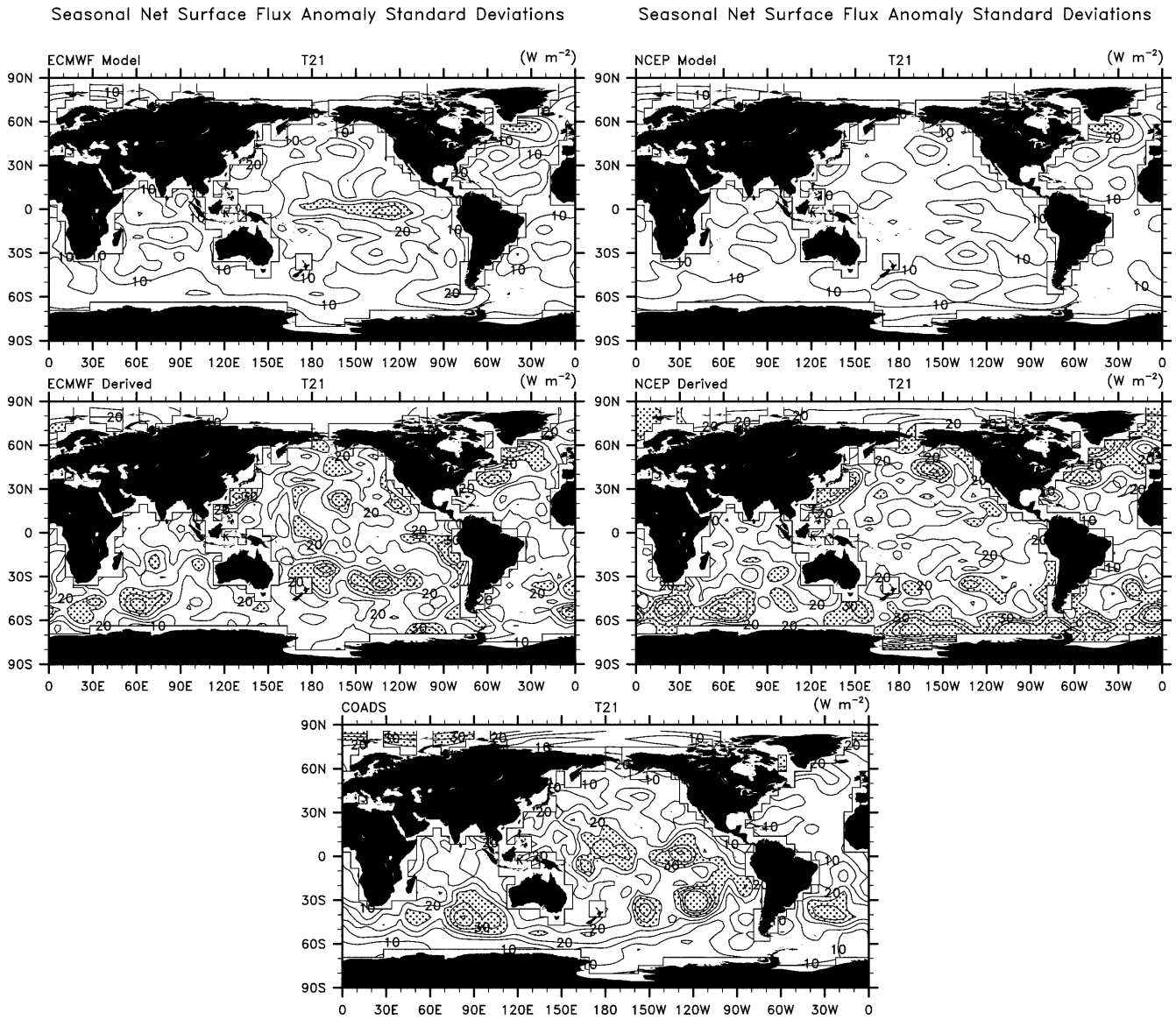

Fig. 7 Standard deviations of seasonal anomalies of the surface fluxes for MAM 1985 to DJF 1988/89, for ECMWF-model, NCEP-model, ECMWF-derived, NCEP-derived, and COADS, in $W\,m^{-2}$ at T21 resolution. The contour interval is 5 $W\,m^{-2}$ and values greater than 25 $W\,m^{-2}$ are stippled

the ocean basin configurations, and the need to smooth the analysis fields to suppress the small scale noise. The same domains and procedures were used for each product. Note that the resulting heat transports from this exercise are *not* indicative of the best estimates that can be made once physical constraints are implemented in conjunction with the uncertainty estimates, which is done in Trenberth and Caron (2001).

Our results for the ERBE period (Fig. 13) show the total implied northward ocean heat transport and also that for the three principal ocean basins. The dividing line between the Atlantic and Indian Ocean is set at 25°E, directly south of Africa. The Atlantic and the Pacific are separated at 70°W, south of South America. For the Pacific and Indian Oceans, we use 130°E from 5°S to south of Australia and 100°E north of 5°S. The Indian and Pacific Ocean partition is confounded by the Indonesian throughflow, so that mass flow in each basin is not closed, and only their sum is meaningful as a heat transport. Nevertheless, the integration of the surface fluxes is the same in each case and thus the breakdown facilitates comparisons. Conservative (i.e., perhaps slightly overestimated) error bars (one standard error) were computed as in Trenberth and Solomon (1994) assuming random errors of 30 $W\,m^{-2}$ over 1000 km scales.

Direct estimates of ocean heat transport are being improved and may provide some guidance in this evaluation. Macdonald (1998) and Macdonald and Wunsch (1996) have made a global inverse analysis of selected high-quality hydrographic sections covering all ocean basins taken prior to the WOCE observational period to

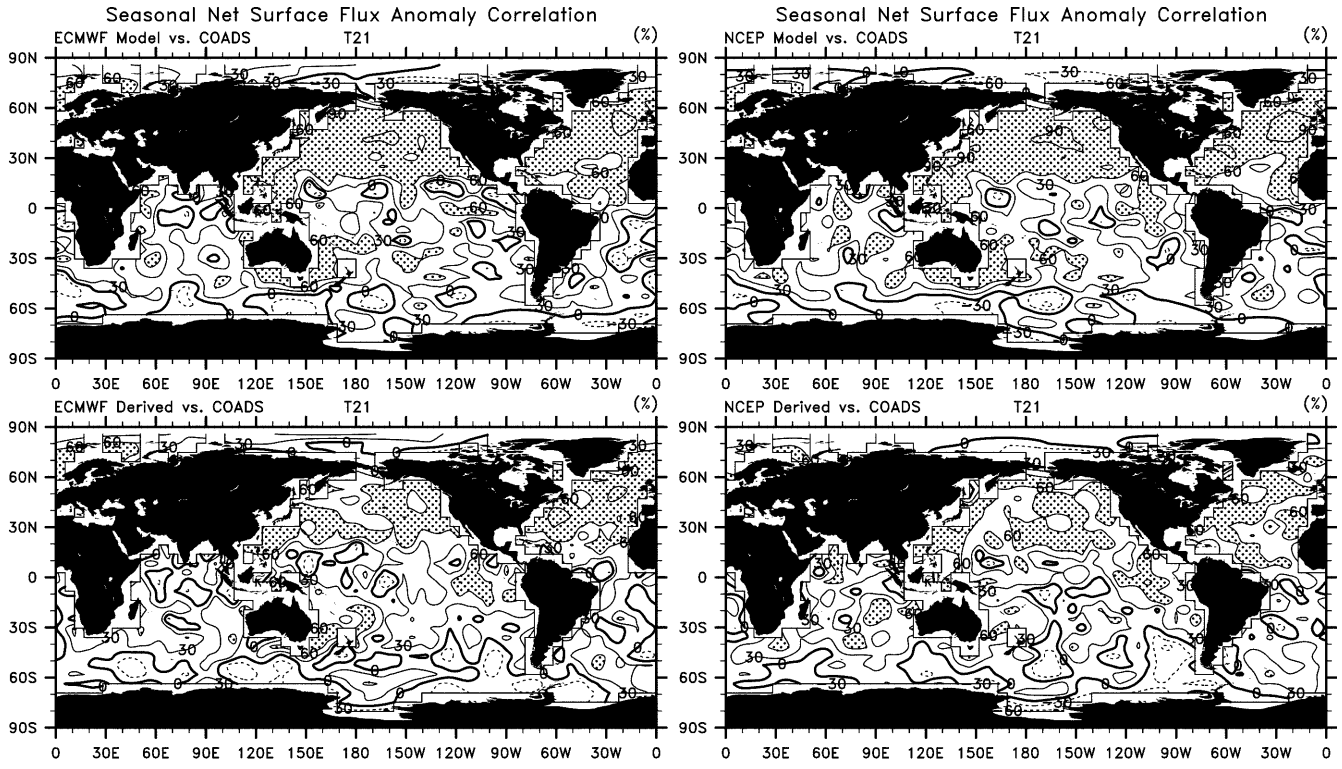

Fig. 8 Seasonal anomaly correlations of the surface fluxes of the ECMWF-model, NCEP-model, ECMWF-derived, NCEP-derived, with COADS in % at T21 resolution. Values greater than 60% are stippled and the contour interval is 30%

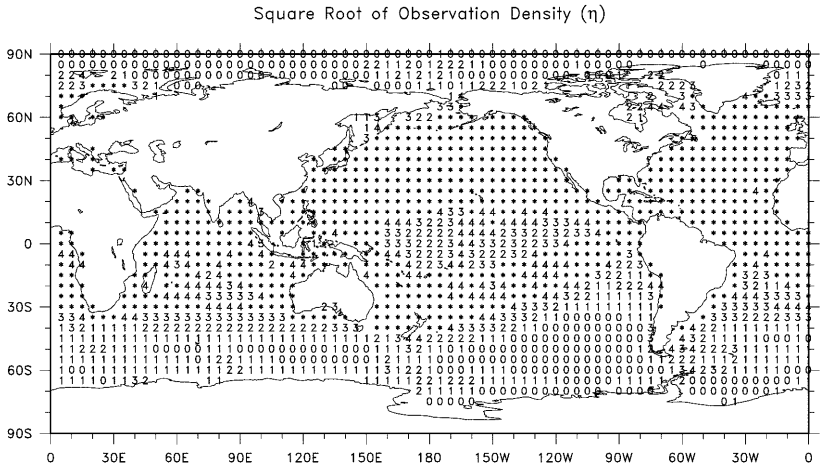

Fig. 9 Map of the square root of the number of observations per month per 5° grid square for COADS from MAM 1985 to DJF 1988/89. All values greater than 4 are indicated by *

produce meridional heat transports. With typical error bars of ±0.3 PW, at 24°N, for the Atlantic Ocean the direct estimates range from about 1.3 PW (Lavin et al. 1998) to 1.1 PW (MacDonald 1998) and for the Pacific: 0.8 PW (Bryden et al. 1991) or 0.5 PW (MacDonald 1998). For the total ocean at 24°N, values range from 1.5 PW (MacDonald and Wunsch 1996) to 2.0 PW from the sum of the Lavin et al. and Bryden et al. values. At 30°S, the total MacDonald and Wunsch (1996) estimate is −0.9 PW. A more comprehensive comparison with these and other direct ocean measurments is given for the derived fields in Trenberth and Caron (2001).

At 24°N, northward heat transports for the total and Atlantic oceans (the Pacific is their difference), respectively, from Fig. 13 are as follows. NCEP-derived (1.7 and 1.0 PW) and COADS (1.9, 1.0 PW) fall within the observational uncertainties, while ECMWF-derived (1.2, 0.7 PW) are a bit low, and the NCEP-model (0.8, 0.6 PW) and ECMWF-model (1.0, 0.7 PW) values are only about half those required. At 30°S values of −0.8 PW for NCEP-derived, −1.1 PW for ECMWF-derived, and −1.3 PW for NCEP-model are within error bars of the direct estimate, while the +1.1 PW for COADS and +1.3 PW for ECMWF-model are well outside of acceptable values.

The total northward heat transport at 68°S, which should be within 0 ± 0.3 PW, instead has global imbalances in PetaWatts of +2.2 for COADS, −2.3 for NCEP-model, +1.1 for ECMWF-model, −0.4 for NCEP-derived and −0.9 for ECMWF-derived products. Note that even though the COADS product was constrained to give zero imbalance, that constraint was for the long-term mean over the entire dataset and does not apply for this ERBE subperiod.

Källberg (1997) has presented the implied net oceanic surface heat transports for each of the 15 years of the ECMWF reanalyses as well as the residual ocean heat transport, integrated from the north (and with reverse sign convention to ours) for the model from 12 to 24 hours into the integration. At 70°S the northward transport ranges from −0.8 PW (in 1979) to 4.4 PW (in 1982). Averaged over all years, the imbalance is 1.3 PW (or 0.9 PW if the two worst years of 1982 and 1986 are excluded), giving a bias in the surface fluxes over the oceans of about −4 W m^{-2} (out of the ocean), consistent with our results for ERBE period. Of these raw products, the two derived ocean heat transports are preferred in terms of the world ocean heat balance and the NCEP-derived is most acceptable. As discussed earlier, the COADS product is seriously flawed south of 20°N and it was tuned to give the "correct" result at 24°N. The model results reveal serious biases throughout the domains. Garnier et al. (1998) came to similar conclusions for the ECMWF model surface fluxes.

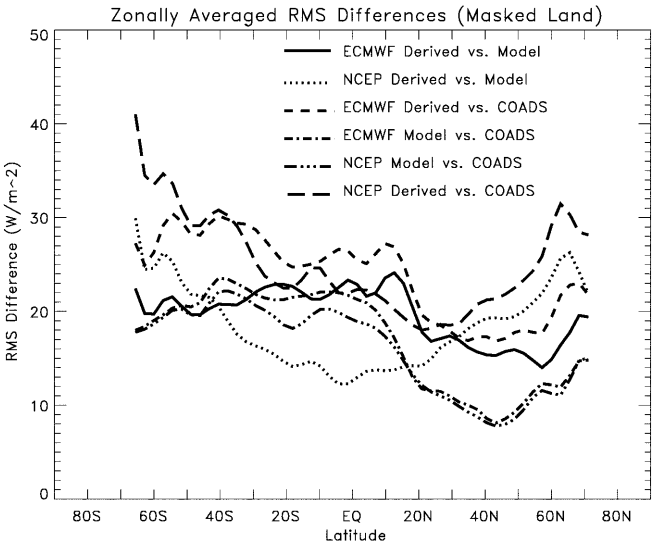

Fig. 10 Zonal mean rms differences of seasonal anomalies among several of the surface flux products in W m^{-2} for the ocean

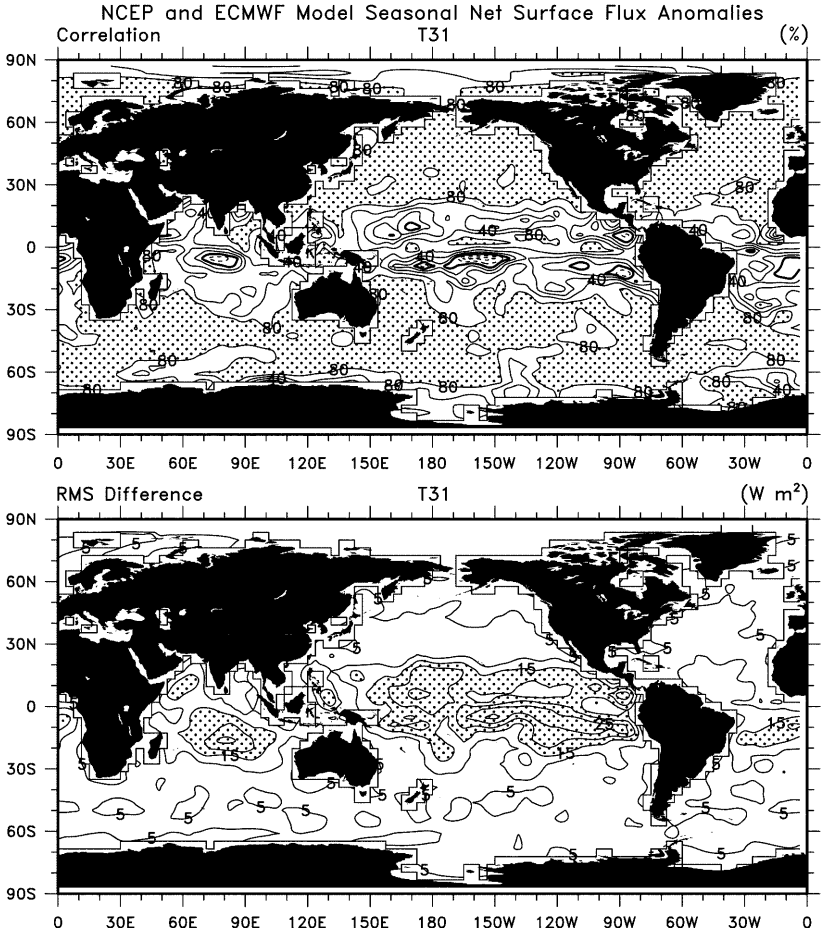

Fig. 11 Correlations % and rms differences in W m^{-2} of the model surface fluxes from ECMWF and NCEP using the seasonal anomalies for MAM 1985 to DJF 1988/89. Correlations greater than 80% are stippled. The contour interval is 20%. For the rms differences the contour interval is 5 W m^{-2} and values exceeding 15 W m^{-2} are stippled

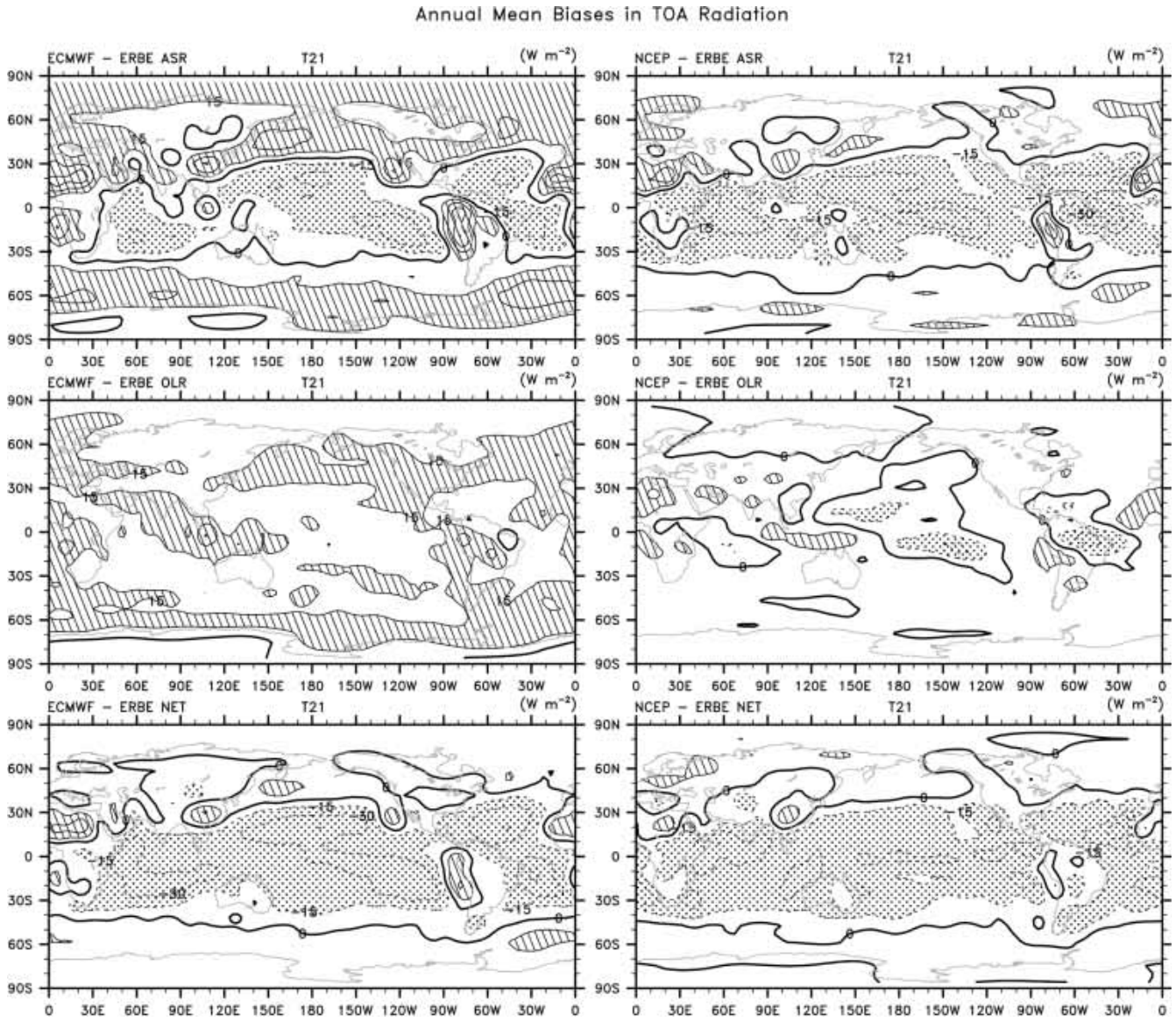

Fig. 12 Annualized biases relative to ERBE of the ECMWF (left panels) and NCEP (right) TOA radiative fluxes from the model for the ASR (top), OLR (center) and net radiation (bottom) at T21 resolution. Values greater than 15 $W\,m^{-2}$ are hatched and less than -15 $W\,m^{-2}$ are stippled, with the contour interval of 15 $W\,m^{-2}$

5 Discussion and conclusions

Comprehensive diagnostic comparisons have been carried out with the NCEP and ECMWF reanalyses of the vertically integrated energy budgets. The new results presented have focussed on the divergence of the atmospheric energy transports and, for the ERBE period, the TOA radiative fluxes and the implied surface fluxes. The latter have been compared with those from the assimilating models and from COADS, both locally and integrated to deduce the implied ocean heat transports.

Although we have tended to focus on how good (or bad) the products are through both mean fields and monthly anomaly time series, it should be emphasized that the ability to even make this assessment represents substantial progress. The broad scale features of the atmospheric energy divergences and the surface fluxes are reproducible and credible. Net fluxes of energy into the ocean in the tropical eastern Pacific exceed 120 $W\,m^{-2}$ in regions where the equatorial dry zone exists. The largest fluxes out of the ocean (>150 $W\,m^{-2}$) are found off the east coasts of Asia and North America over the Kuroshio and Gulf Stream and patterns are quite similar. Large fluxes into the ocean in the tropical Indian Ocean and over parts of the southern ocean, North Pacific and tropical Atlantic are also reproducible. Consequently it is the details of the magnitudes and systematic biases that are now of main concern.

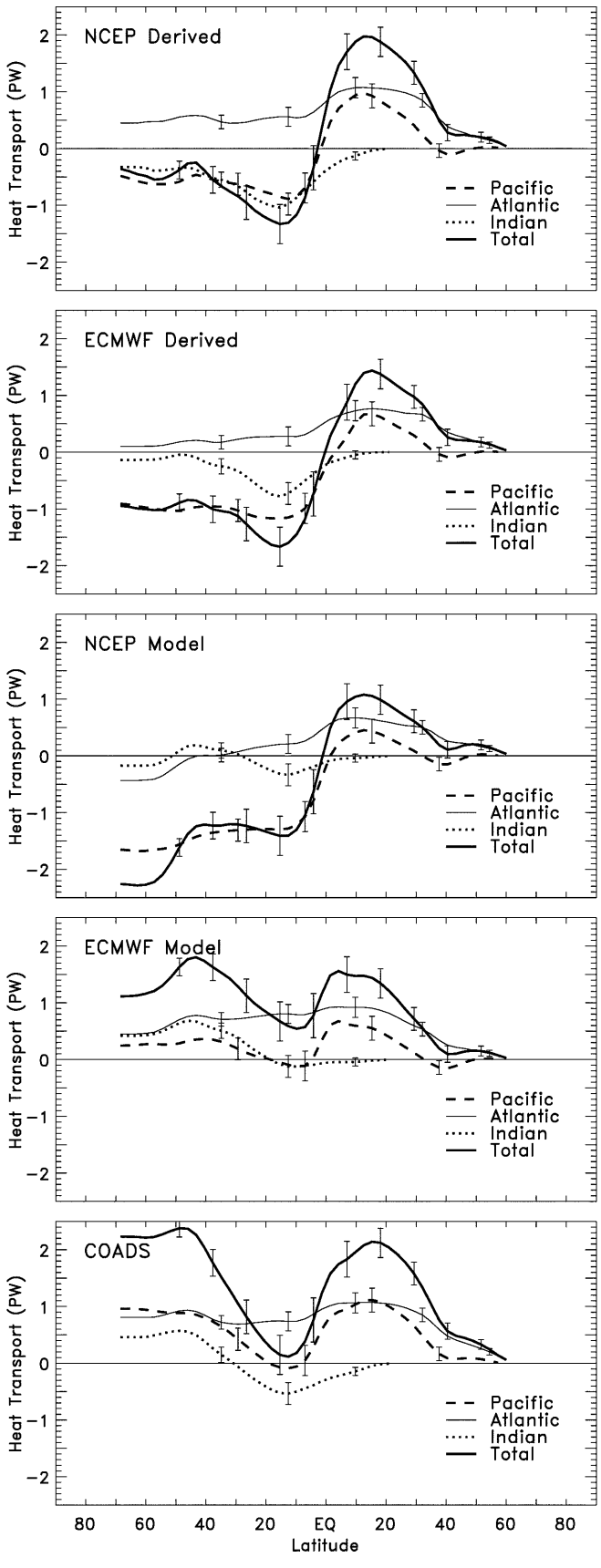

Fig. 13 Implied zonal annual mean ocean heat transports starting at 0 at 65°N based upon the surface fluxes for February 1985 to April 1989 for the total, Atlantic, Indian and Pacific basins for NCEP-derived, ECMWF-derived, NCEP-model, ECMWF-model, and COADS in PetaWatts (PW). One standard error bars are indicated

However, the evaluation highlights the poor results over land, and especially in and around high topography. Local imbalances indicate rms errors in the divergence of the atmospheric energy transports on scales of 500 km or so (T31) often of about 30 $W m^{-2}$ generally over land in both reanalyses and >50 $W m^{-2}$ over Antarctica and complex topography, more notably in the NCEP reanalyses. Generally there is a poor correspondence in time series over land, as expected, because any common signal should be very small.

The picture is somewhat better over the oceans in the extratropics where the results from the two reanalyses agree much better in their time series, with correlations exceeding 0.7 for the derived products. Rms differences of about 40 $W m^{-2}$ for monthly values imply errors of 25 to 30 $W m^{-2}$ most places on about 500 km scales although embedded within a signal of about 40 $W m^{-2}$ in the extratropics for monthly means. There is no useful common signal in the tropics at these scales. Although bulk flux seasonal anomalies from the models and COADS agree very well over the northern extratropical oceans, with rms differences between the two model fluxes of 5 to 10 $W m^{-2}$, both products contain large systematic biases which make them unsuitable for determining ocean heat transports.

The integrated framework of computing surface fluxes using direct estimates as well as from those derived from the energy budget has also been exploited by Curry et al. (1999) for the TOGA COARE IOP. In their case the in situ estimates every three hours at 50 km resolution consist of direct measurements and bulk fluxes. One key result is that high frequency, diurnal and small scale variability, if not resolved, is a source of error. Largest errors and uncertainties occur in the net shortwave flux where rms errors of daily mean ship versus satellite estimates are 35 $W m^{-2}$. ECMWF net surface fluxes were found to have a bias of 37 $W m^{-2}$ and rms error of 79 $W m^{-2}$ compared with the satellite estimates. Imbalances with the energy budgets reveal 41 $W m^{-2}$ biases of which perhaps 34 $W m^{-2}$ may arise from the net shortwave. Biases in radiosonde measurements (especially of moisture) may account for 10% of the errors (Johnson and Ciesielski 1999). These results help explain and are consistent with the global monthly mean results of our analysis.

The PAOBS problem discussed in Sect. 2 is likely to have affected both the model and derived fluxes over the southern oceans. Accordingly, the NCEP surface fluxes should be discounted to some extent south of about 30°S and error bars increased. A small adjustment over this region can easily bring the derived northward ocean heat transports to about zero at 70°S and therefore satisfy

physical constraints, and this exercise is done in Trenberth and Caron (2001).

In the tropics, the problems outlined by Trenberth et al. (2001) associated with changes in the observing system, particularly satellite data, adversely influence the ECMWF results. Shortcomings in the hydrological cycle in the NCEP reanalyses in the tropics suggest that these too have limitations, although there is huge compensation between the budgets for dry static energy and the moist component, so that the total is more robust (Trenberth and Solomon 1994). However, the lack of reproducibility where strong convection is active and extensive stratocumulus decks dominate suggests that these are key areas where atmospheric processes are not well replicated.

The northward ocean heat transports computed as residuals of the various surface heat fluxes highlight the need for physical constraints to be utilized to the fullest extent. The model surface fluxes are biased, especially because of difficulties with clouds in the radiative components and spin up of precipitation and evaporation. COADS products of time series of the surface fluxes are shown to be unreliable where the number of monthly observations per 5° square are less than about 25, and thus anomalies are of limited value south of 20°N. The surface fluxes derived from the TOA radiation plus atmospheric heat transports are more consistent but differ from one another with magnitudes that imply error bars of a few tenths PW. Largest uncertainties occur over data sparse areas, and values over the tropics and southern oceans are the most uncertain.

The ocean heat transports were computed without regard to changes in ocean heat storage, which is not neglible from year to year, although it is a reasonable assumption for the four years or so we used here. Sun and Trenberth (1998) presented the complete results of the surface energy budget, including the changes in ocean heat storage for the ERBE period for the Pacific Ocean using the NCEP-derived atmospheric energy divergences, and demonstrated the large effects of the 1986–87 El Niño and the 1988–89 La Niña.

The results of this work have emphasized the conclusions of Yu et al. (1999) who found the various datasets to be physically inconsistent with one another. This clearly calls into question the parameterized model fluxes at the TOA and the surface, although further advances are also needed in the mass, moisture and energy transports in the analysed atmosphere. This study highlights the need for these quantities to be examined in the context of the physical constraints. Although tremendous strides have been made through the reanalyses, future reanalyses are expected to greatly improve upon the various problems that have been encountered with the first attempts from both centers.

Acknowledgments This research was sponsored by NOAA Office of Global Programs grant NA56GP0247 and the joint NOAA/NASA grant NA87GP0105. Many thanks to Jim Hurrell for comments.

References

Alexander MA, Schubert SD (1990) Regional earth-atmosphere energy balance estimates based on assimilations with a GCM. J Clim 3: 15–31

Annamalai H, Slingo JM, Sperber KR, Hodges K (1999) The mean evolution and variability of the Asian summer monsoon: Comparison of ECMWF and NCEP-NCAR reanalyses. Mon Wea Rev 127: 1157–1186

Boer GJ, Sargent NE (1985) Vertically integrated budgets of mass and energy of the globe. J Atmos Sci 42: 1592–1613

Bryden HL, Roemmich DH, Church JA (1991) Ocean heat transport across 24°N in the Pacific. Deep-Sea Res 38: 297–324

Curry JA, Clayson CA, Rossow WB, Reeder R, Zhang Y-C, Webster PJ, Liu G, Sheu R-S (1999) High-resolution satellite-derived dataset of the surface fluxes of heat, freshwater, and momentum for the TOGA COARE IOP. Bull Amer Meteor Soc 80: 2059–2080

da Silva AM, Young CC, Levitus S (1994) Atlas of Surface Marine Data 1994 Volume 1: Algorithms and Procedures, NOAA Atlas NESDIS 6, U.S. Dept. Commerce, Washington DC, 83 pp

Garnier E, Barnier B, Béranger K, Siefridt L (1998) Global ocean thermohaline forcing from 15 years of ECMWF reanalyses. Proc. First WCRP Intl. Conf. on Reanalyses, Silver Spring MD. 27–31 October, 1997, WCRP-104, WMO/TD-876, pp 57–60

Gibson JK, Kållberg P, Uppala S, Hernandez A, Nomura A, Serrano E (1997) ERA description. ECMWF Reanalysis Proj. Rep. 1., 72 pp

Gleckler PJ, Weare BC (1997) Uncertainties in global ocean surface heat flux climatologies derived from ship observations. J Clim 10: 2764–2781

Hurrell JW, Trenberth KE (1996) Satellite versus surface estimates of air temperature since 1979. J Clim 9: 2222–2232

Johnson RH, Ciesielski PE (1999) Rainfall and radiative heating rate estimates from TOGA COARE atmospheric budgets. J Atmos Sci 53: 1838–1855

Josey SA, Kent EC, Taylor PK (1999) New insights into the ocean heat budget closure problem from analysis of the SOC air-sea flux climatology, J Clim 12: 2856–2880

Kalnay E, Kanamitsu M, Kistler R, Collins W, Deaven D, Gandin L, Iredell M, Saha S, White G, Woollen J, Zhu Y, Chelliah M, Ebisuzaki W, Higgins W, Janowiak J, Mo K-C, Ropelewski C, Leetmaa A, Reynolds R, Jenne R (1996) The NCEP/NCAR Reanalysis Project. Bull Amer Meteor Soc 77: 437–471

Kållberg P (1997) Aspects of the reanalysed climate. ECMWF Reanalysis Proj. Rep 2. 89 pp

Lavin A, Bryden HL, Parrilla G (1998) Meridional transport and heat flux variations in the subtropical North Atlantic, Global Atmos Ocean Syst 6: 269–293

Macdonald AM (1998) The global ocean circulation: A hydrographic estimate and regional analysis. Prog Oceanogr 41: 281–382

Macdonald AM, Wunsch C (1996) An estimate of global ocean circulation and heat fluxes. Nature 382: 436–439

Mo K-C, Higgins RW (1996) Large-scale atmospheric moisture transport as evaluated in the NCEP/NCAR and the NASA/DAO reanalyses. J Clim 9: 1531–1545

Stendel M, Arpe K (1997) Evaluation of the hydrological cycle in reanalyses and observations. Max Planck Institut für Meteorologie Rep 228. 52 pp

Sun D-Z, Trenberth KE (1998) Coordinated heat removal from the tropical Pacific during the 1986–87 El Niño. 25: 2659–2662

Trenberth KE (1991) Climate diagnostics from global analyses: conservation of mass in ECMWF analyses. J Clim 4: 707–722

Trenberth KE (1997) Using atmospheric budgets as a constraint on surface fluxes. J Clim 10: 2796–2809

Trenberth KE (1998) The heat budget of the atmosphere and ocean. Proc. First WCRP Intl. Conf. on Reanalyses, Silver

Spring MD. 27–31 October, 1997, WCRP-104, WMO/TD-876, pp 17–20
Trenberth KE, Guillemot CJ (1995) Evaluation of the global atmospheric moisture budget as seen from analyses. J Clim 8: 2255–2272
Trenberth KE, Guillemot CJ (1998) Evaluation of the atmospheric moisture and hydrogical cycle in the NCEP/NCAR reanalyses. Clim Dyn 14: 213–231
Trenberth KE, Solomon A (1994) The global heat balance: heat transports in the atmosphere and ocean. Clim Dyn 10: 107–134
Trenberth KE, Berry JC, Buja LE (1993) Vertical interpolation and truncation of model-coordinate data. NCAR Technical Note NCAR/TN-396 + STR, 54 pp
Trenberth KE, Christy JR, Hurrell JW (1992) Monitoring global monthly mean surface temperatures. J Clim 5: 1405–1423
Trenberth KE, Hurrell JW, Solomon A (1995) Conservation of mass in three dimensions. J Clim 8: 692–708
Trenberth KE, Stepaniak DP, Caron JM (2000) The global monsoon as seen through the divergent atmospheric circulation. J Clim 13: 3969–3993
Trenberth KE, Stepaniak DP, Hurrell JW, Fiorino M (2001) Quality of reanalyses in the tropics. J Clim 14: (in press)
Trenberth KE, Caron JM (2001) Estimates of meridional atmosphere and ocean heat transports. J Clim (submitted)
Uppala S (1997) Observing system performance in ERA. ECMWF Reanalysis Proj. Rep 3. 261 pp
Woodruff SD, Slutz RJ, Jenne RL, Steurer PM (1987) A comprehensive ocean-atmosphere data set. Bull Amer Meteor Soc 68: 1239–1250
Yanai M, Tomita T (1998) Seasonal and interannual variability of atmospheric heat sources and moisture sinks as determined from NCEP-NCAR reanalyses. J Clim 11: 463–482
Yang S-K, Hou Y-T, Miller AJ, Campana KA (1999) Evaluation of the Earth radiation budget in NCEP-NCAR reanalysis with ERBE. J Clim 12: 477–493
Yu R, Zhang M, Cess RD (1999) Analysis of the atmospheric energy budget: a consistency study of available data sets. J Geo Phys Res 108: 9655–9661

Appendix: Diagnostic fields

The reanalyses from both centers have been used to compute the vertically-integrated mass, moisture, heat, and energy budgets for the atmosphere. The full resolution data four-times daily on model coordinates are used to obtain the best accuracy possible. The processing of the 15 years 1979 to 1993 of ECMWF ERA analyses on 31 model levels at T106 resolution 4 times per day has taken a major effort. To process one month of data required 8 hours of time on an SGI machine (SGI Power Challenge XL 10000; 8 processors and 1 Gb of memory), largely because of the huge volumes of input and output required.

We have similarly processed all the NCEP and ECMWF pressure level data, which are more readily available, on a 2.5° grid at 17 levels to provide products that can be compared with the complete results and evaluated to determine the effects of degraded horizontal and vertical resolution on the results. These will be reported on elsewhere.

We processed 3 Terabytes of data in 1999, mainly from the ECMWF reanalyses, and the output of derived products occupy about 5.2 Gigabytes for the pressure level data and a further 24.5 Gigabytes for the model level data. Vertical integrals of the following fields are archived (the abbreviated name on the archive is also given):

Fields of variables and their tendencies:	
Mass, Surface pressure	PS
Kinetic Energy	KE
Total Energy: $(C_pT + Lq + gZ_s + k)$	TE
Precipitable Water	PW
Precipitable Water Tendency	QTEN
Total Energy Tendency	TETEN
Transports:	
Mass: zonal	U
Mass: meridional	V
Heat: Zonal Component	UT
Heat: Meridional Component	VT
Moisture: Zonal Component	UQ
Moisture: Meridional Component	VQ
Kinetic Energy: Zonal Component	UK
Kinetic Energy: Meridional Component	VK
Geopotential: Zonal Component	UZ
Geopotential: Meridional Component	VZ
From which we compute:	
Evaporation minus Precipitation (E-P)	EP
Mass Residual	MRES
Total Energy Divergence	TEDIV
Dry Static Energy Divergence	DSEDIV
Latent Heat Divergence	LEDIV
Diabatic Heating minus Frictional Heating	Q1QF
Net Downward Radiation, Top of Atmosphere	RAD
Net Upward Heat Flux, Surface	FS

Full documentation of the derived products is at **http://www.cgd.ucar.edu/cas/catalog/tn430/** from which it is possible to migrate to either the full listings of ECMWF or NCEP derived products, and all of these fields are available through ftp directories which are specified on the web pages for each dataset. The data can be downloaded either from the web browser or by standard anonymous ftp. The products are all global T42 single level vertically-averaged grids as individual monthly mean time series from 1979 through 1993, and monthly, seasonal and yearly averages (climatologies). For NCEP the processing continues using products from the Climate Data Assimilation System, currently through 1995.